

# Scaling-up Remote Sensing Segmentation Dataset with Segment Anything Model

Di Wang<sup>1</sup> Jing Zhang<sup>2</sup> Bo Du<sup>1</sup> Dacheng Tao<sup>2</sup> Liangpei Zhang<sup>3</sup>

<sup>1</sup>School of Computer Science, Wuhan University

<sup>2</sup>School of Computer Science, Faculty of Engineering, The University of Sydney

<sup>3</sup>LIESMARS, Wuhan University

{d.wang, dubo, zlp62}@whu.edu.cn; jing.zhang1@sydney.edu.au; dacheng.tao@gmail.com

## Abstract

The success of the Segment Anything Model (SAM) demonstrates the significance of data-centric machine learning. However, due to the difficulties and high costs associated with annotating Remote Sensing (RS) images, a large amount of valuable RS data remains unlabeled, particularly at the pixel level. In this study, we leverage SAM and existing RS object detection datasets to develop an efficient pipeline for generating a large-scale RS segmentation dataset, dubbed SAMRS. SAMRS surpasses existing high-resolution RS segmentation datasets in size by several orders of magnitude, and provides object category, location, and instance information that can be used for semantic segmentation, instance segmentation, and object detection, either individually or in combination. We also provide a comprehensive analysis of SAMRS from various aspects. We hope it could facilitate research in RS segmentation, particularly in large model pre-training. The code and dataset will be available at SAMRS<sup>1</sup>.

## 1. Introduction

The advancement of earth observation technologies has led to the generation of abundant remote sensing images (RSI). These images retain valuable information about the spatial distribution and condition of extensive ground surfaces and geospatial objects, and can be conveniently accessed in real-time. Consequently, remote sensing data has garnered the interest of various disciplines, including agricultural monitoring, urban planning, and environmental protection. In particular, the identification of surface targets has been a fundamental task in these fields for several years.

To our knowledge, a significant number of RSIs remain unlabeled. Unlike natural images that can be easily comprehended by the human eye, interpreting RSI taken from an aerial perspective typically demands specialized expertise

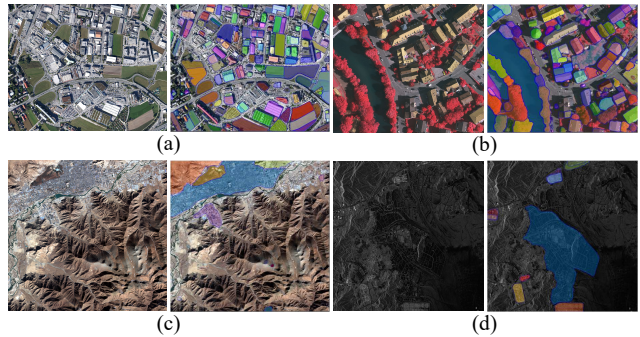


Figure 1. Some examples of SAM segmentation results on RSIs: (a) RGB aerial image obtained from the IsAID dataset [17]. (b) Airborne aerial image composed of near-infrared, red, and green bands. This image is from the ISPRS Vaihingen dataset<sup>2</sup>. (c) RGB satellite image observed by GF-2 sensors. This image is from the GID dataset [12]. (d) Hisea-1 SAR image from the Marine Farms Segmentation track of the 5th Gaofen Challenge<sup>3</sup>.

from practitioners. Furthermore, RSI objects are often distributed sparsely, and the images frequently contain small targets, making the labeling process less efficient. Therefore, the annotation of RSI has traditionally required substantial labor and time costs. Among various RS tasks, the classification task requires only a single category for the entire scene, and the detection task involves the additional step of bounding box annotation, while segmentation is particularly challenging since it necessitates pixel-level annotations to accurately delineate object boundaries.

Do we have to spend a significant amount of time annotating RSIs? The answer is probably no. Recently, the segment anything model (SAM) [6], which excels in object segmentation, has gained popularity as a new research focus in the field of computer vision. SAM accurately captures object locations and contours (*i.e.*, in the form of masks), enabling it to distinguish various objects in the foreground

<sup>2</sup><https://www.isprs.org/education/benchmarks/UrbanSemLab/2d-sem-label-vaihingen.aspx>

<sup>3</sup><https://www.gaofen-challenge.com/challenge>

<sup>1</sup>Preprint. Work in progress.

and background. Furthermore, SAM possesses an impressive zero-shot segmentation ability, exhibiting high performance even when applied to specialized scenarios such as cell images photographed by microscopes [4] and medical images [10], despite being trained on a vast dataset of natural images. We have also found it performs well in recognizing diverse targets in RSI, even when the images are obtained using sensors that perceive different bands, such as infrared and microwave, or with varying resolutions, such as airborne or satellite imagery, as illustrated in Figure 1. Although we acknowledge that SAM may not have fully detected all regions, we believe that it has significant potential to improve the efficiency of annotating RSIs since it delivers promising segmentations on recognized areas.

Therefore, in this study, we aim to utilize SAM to efficiently construct a large-scale RS segmentation dataset by obtaining pixel-level annotations for RSIs. Ground objects in RSI possess definite category properties, which are essential for real RS recognition tasks. However, the segmentation maps produced by SAM lack such information, rendering them unsuitable for labeling RSIs. To address this issue, we notice the annotations in existing RS object detection datasets, which include category and bounding box information. With the aid of SAM, we can leverage such detection annotations to obtain pixel-level semantic labels and efficiently construct large-scale segmentation datasets. To the best of our knowledge, it is the first time that SAM has been employed for labeling RSIs. We hope this research could significantly enhance the annotation efficiency of RSIs, thereby unlocking the full potential of RS models, especially in the context of segmentation tasks.

## 2. Implementation

### 2.1. Segment Anything Model

To perform segmentation, additional prompts are needed to guide SAM to locate the object of interest, in addition to the input image. SAM supports various prompts, such as points, boxes, and masks, which can be input into the model either alone or in combination. It is important to note that when using point prompts, it is necessary to indicate whether the points are foregrounds or backgrounds. In this study, we use detection annotations from existing datasets to obtain all kinds of prompts since they contain both location and category information.

### 2.2. Datasets

In this study, we employ SAM on four different RS object detection datasets, namely HRSC2016 [8], DOTA-V2.0 [5], DIOR [7], and FAIR1M-2.0 [1]. HRSC2016 is primarily designed for ship detection and comprises only one category. In comparison to the other three datasets, it has the smallest data volume. Additionally, in the testing set, 124

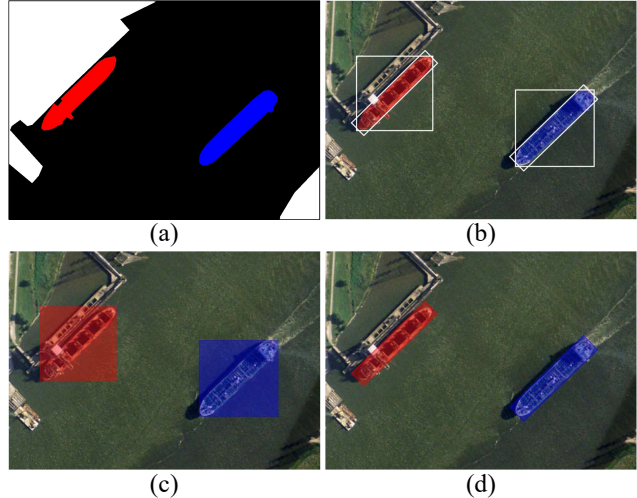


Figure 2. The differences between segmentation labels and mask prompts. (a) Pixel-level annotated map from the original dataset. (b) Pixel-level annotations along with horizontal and rotated box ground truths. (c) Mask prompts derived from horizontal boxes. (d) Mask prompts derived from rotated boxes. The ship instances are marked with different colors by following (a).

images possess bounding box annotations and pixel-level labels simultaneously, making it highly suitable for evaluating the accuracy of SAM annotations. Therefore, we conduct an ablation study on the testing set consisting of the aforementioned 124 images to determine the optimal configuration for SAM. Following this, we generate segmentation labels for the remaining datasets. To obtain a segmentation dataset with more images or categories, we opt for the latest versions of DOTA and FAIR1M. Based on the available annotations, we only transform the training and validation sets of DOTA-V2.0 and FAIR1M-2.0, while for DIOR, all data has been utilized.

### 2.3. Prompt Settings

As RSIs are captured from an overhead perspective, the objects in them can have arbitrary orientations, unlike natural image objects that are typically oriented upward due to gravity. Hence, in addition to the usual horizontal bounding boxes (H-Box), we also consider oriented bounding boxes or rotated bounding boxes (R-Box) as box prompts. However, SAM does not directly support R-Box prompts. To address this issue, we use the minimum circumscribed horizontal rectangle of the R-Box, which is denoted as “RH-Box”. It is also worth noting that the instances in the HRSC2016 testing set contain both H-Box and R-Box ground truth annotations.

In the case of the point prompt, due to the intricate shapes of various RS objects, such as airplanes, we have taken a cautious approach and only consider the center point

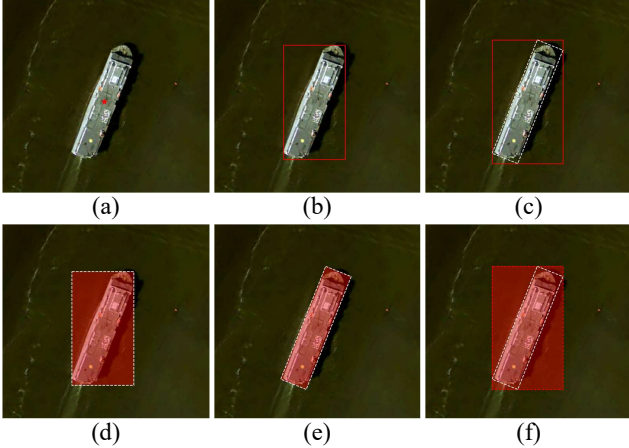


Figure 3. The adopted basic prompts. (a) CP. (b) H-Box. (c) RH-Box. (d) H-Box-M. (e) R-Box-M. (f) RH-Box-M. The dashed line is used for the convenience of visualization.

as the foreground. We did not include background points in our study, as accurately defining them in an automated way can be challenging without additional contextual information. Regarding the mask prompt, we define the region enclosed by corresponding boxes as the mask prompt. Figure 2 illustrates the differences between the adopted mask prompts and ground truth segmentation labels. In SAM, the mask is a single-channel score matrix where positive values denote the active area where the target is located, whereas negative values represent irrelevant areas. In our experiments, we assign the values in these two types of areas as 1,000 and -1,000, respectively.

In summary, we have obtained six basic prompts, namely center point (CP), H-Box, RH-Box, and their corresponding masks, *i.e.*, H-Box-M, R-Box-M, and RH-Box-M, as illustrated in Figure 3.

## 2.4. Ablation Study

In addition to the above basic prompts, we also investigate various combinations of prompts in this study. To conduct a comprehensive analysis, we compute two types of mean intersection over union (mIOU) metrics:  $mIOU_I$  and  $mIOU_P$ , which measure the similarity between the predicted segmentation mask and the ground truth label. The former is the average value of the IoU calculated on a per-instance basis, while the latter measures the pixel-level accuracy. Given the  $i$ th instance with intersection set  $I_i$  and union set  $U_i$ , and the number of instances  $N$ , we have:

$$mIOU_I = \frac{1}{N} \sum_{i=1}^N \frac{I_i}{U_i} \quad mIOU_P = \frac{\sum_{i=1}^N I_i}{\sum_{i=1}^N U_i}. \quad (1)$$

Table 2 presents the evaluation results of utilizing different prompts. The point prompt delivers the worst performance and negatively affects the accuracy of any prompt

Table 1. Results of using different prompts on the HRSC2016 testing set consisting of 124 images.

CP	H-Box	H-Box-M	R-Box-M	RH-Box	RH-Box-M	$mIOU_I$	$mIOU_P$
<b>Point</b>							
✓						16.14	2.72
<b>H-Box</b>							
	✓					<b>89.97</b>	<b>79.40</b>
		✓				40.54	36.71
✓	✓					86.67	77.35
		✓				74.21	62.25
✓						24.54	5.41
✓	✓	✓				59.71	49.30
<b>R-Box</b>							
			✓			<b>65.54</b>	<b>59.78</b>
✓			✓			26.49	4.97
<b>RH-Box</b>							
				✓		<b>88.85</b>	<b>76.42</b>
					✓	34.63	31.81
✓				✓		83.55	72.67
				✓	✓	66.23	52.75
✓					✓	23.71	5.10
✓				✓	✓	49.24	39.03

combinations. This could be attributed to the insufficient amount of foreground points, which cannot guide the model effectively. The mask prompt performs better than the point prompt, but it still cannot generate high-quality segmentation annotations. The highest accuracy achieved by a mask prompt is approximately 60%, which is still much lower than the optimal prompts. Furthermore, the mask prompt has a negative impact on the performance of box prompts. When solely adopting the H-Box prompt, we obtain the highest accuracy compared to the point and mask prompts. For the case of utilizing R-Box annotations, the RH-Box prompt also achieves satisfactory performance. From this experiment, we conclude that: *if an RS object detection dataset only has R-Box annotations, then the RH-Box prompt should be used; otherwise, the H-Box prompt should be adopted.* This consideration is applied in our later dataset transformations.

## 2.5. Dataset Transformation

For the FAIR1M-2.0 dataset, since it only contains R-Box annotations, we use the corresponding RH-Box as the prompt. For DOTA-V2.0 and DIOR, we directly adopt the H-Box prompt. Prior to transformation, we follow the common practice to crop images in DOTA and FAIR1M datasets to  $1,024 \times 1,024$  and  $600 \times 600$ , respectively, while images in DIOR are maintained at the size of  $800 \times 800$ . The resulting datasets are named SOTA (*i.e.*, DOTA  $\rightarrow$  SOTA), SIOR (*i.e.*, DIOR  $\rightarrow$  SIOR), and FAST (*i.e.*, Fine-grAined object recognItion in high-Resolution remote sensing imagery  $\rightarrow$  Fine-grAined Segmentation for high-resolution remoTe sensing imagery), respectively. These datasets constitute a comprehensive and large-scale remote sensing segmentation database, named SAMRS, which is short for Segment Anything Model annotated Remote Sens-

<sup>4</sup><https://www.isprs.org/education/benchmarks/UrbanSemLab/2d-sem-label-potsdam.aspx>

Table 2. Comparisons of different high-resolution RS segmentation datasets.

Dataset	#Images	#Category	#Channels	Resolution (m)	Image size	Instance	Fine-grained
ISPRS Vaihingen <sup>2</sup>	33	6	IR,R,G	0.09	2,494 × 2,064		
ISPRS Potsdam <sup>4</sup>	38	6	IR,RGB	0.05	6,000 × 6,000		
Zurich Summer [13]	20	8	NIR,RGB	0.62	1,000 × 1,150		
Zeebruges [11]	7	8	RGB	0.05	10,000 × 10,000		
DeepGlobe Land Cover [3]	1,146	7	RGB	0.5	2,448 × 2,448		
UAVid [9]	420	8	RGB	-	4,096 × 2,160 or 3,840 × 2,160		
GID [12]	150	15	NIR,RGB	1 or 4	6,800 × 7,200		
Landcover.ai [2]	41	3	RGB	0.25 or 0.5	9,000 × 9,500 or 4,200 × 4,700		
IsAID [17]	2,806	15	RGB	-	800 × 800 ~ 4,000 × 13,000	✓	
LoveDA [16]	5,987	7	RGB	0.3	1,024 × 1,024		
<b>SAMRS</b>							
<b>SOTA</b>	17,480	18	RGB	-	1,024 × 1,024	✓	
<b>SIOR</b>	23,463	20	RGB	-	800 × 800	✓	
<b>FAST</b>	64,147	37	RGB	-	600 × 600	✓	✓

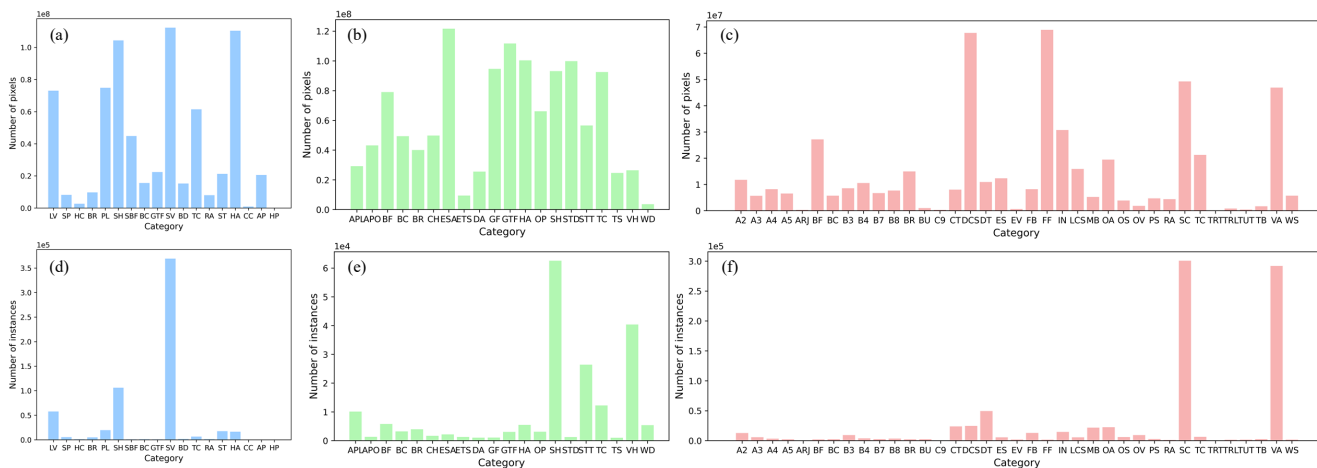


Figure 4. Statistics of the number of pixels and instances for each category in the SAMRS database. The histograms for the subsets SOTA, SIOR, and FAST are shown in the first, second, and third columns, respectively. The first row presents histograms on a per-pixel basis, while the second row presents histograms on a per-instance basis. A list of category abbreviations is provided in the appendix.

ing Segmentation Database.

### 3. SAMRS

#### 3.1. Basic Information

We present the comparison of our SAMRS dataset with existing high-resolution RS segmentation datasets in Table 2 from different aspects. Based on the available high-resolution RSI object detection datasets, we can efficiently annotate 10,5090 images based on SAM and the identified prompt settings (Sec. 2.4), which is more than ten times the capacity of existing datasets. Additionally, SAMRS inherits the categories of the original detection datasets, which makes them more diverse than other high-resolution RS segmentation collections. It is worth noting that RS object datasets usually have more diverse categories than RS segmentation datasets due to the difficulty of tagging pixels in RSIs, and thus our SAMRS reduces this gap.

Specifically, the resulting FAST dataset is a large-scale fine-grained RS segmentation dataset that targets diverse vehicles and grounds, while SOTA and SIOR are segmentation datasets containing common object categories. For this reason, we did not unify their categories. In addition to the massive pixel-level semantic mask annotations, SAMRS includes instance mask and bounding box annotations. This means that *it can be used to perform semantic segmentation, instance segmentation, and object detection, either individually or in combination, particularly in the context of large model pre-training [14, 15]*. This feature sets SAMRS apart from the IsAID dataset, which was independently annotated from scratch on DOTA-V1.0 [18] images.

#### 3.2. Statistics and Analysis

To gain a deeper understanding of the characteristics of the SAMRS dataset, we conduct a thorough analysis of their capacity per category, including pixel and instance num-

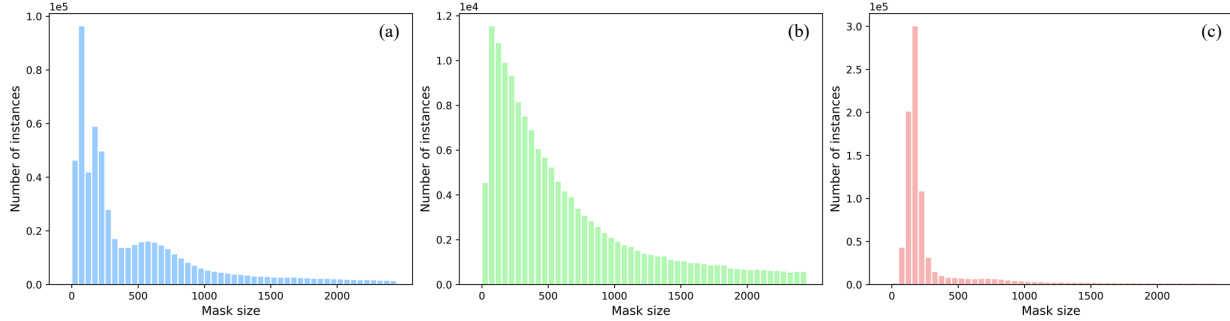


Figure 5. Statistics of the mask sizes in different subsets of the SAMRS database. (a) SOTA. (b) SIOR. (c) FAST.

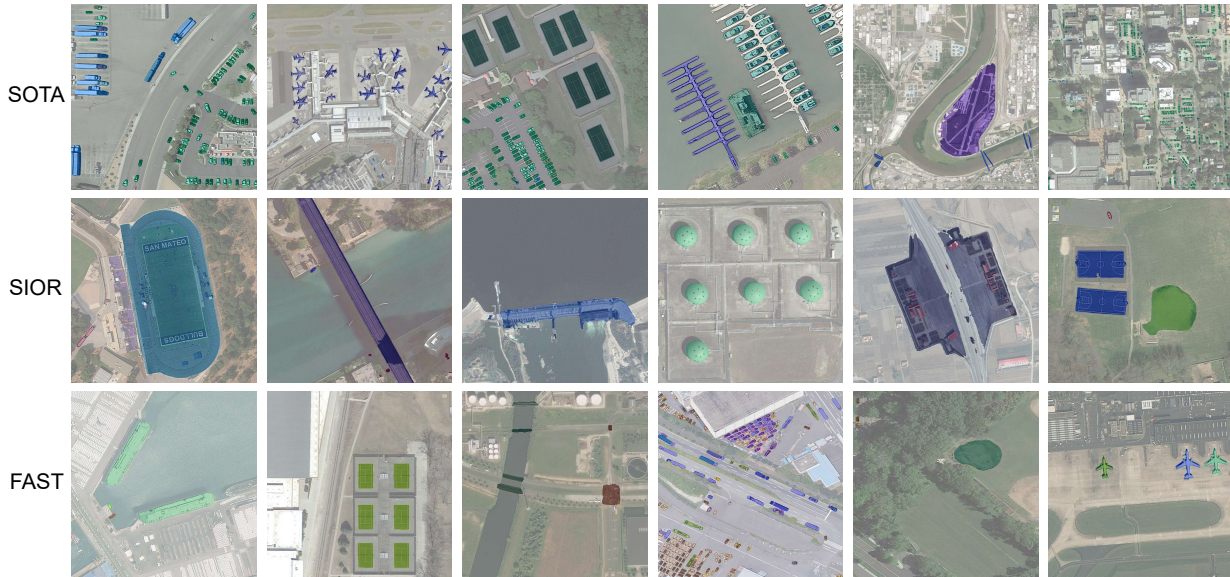


Figure 6. Some visual examples from the three subsets of our SAMRS dataset.

bers. The results are presented in Figure 4. In this analysis, we only count instances that have valid masks. The figure indicates that SIOR has more balanced categories compared to SOTA and FAST. In the instance-level statistics, we observe a large number of vehicle annotations, particularly on small ships and cars, as they are common in the real world and frequently appear in RSIs. This could also be the goal of initially developing these detection datasets. For instance, DOTA-V2.0 focuses on small targets, while FAIR1M mainly aims to accurately distinguish between different types of vehicles. Furthermore, it is observed that some categories have a high number of pixels but a low number of instances, which is likely due to their large size. For instance, the *expressway-service-area* in SIOR and the *football-field* in FAST demonstrate this pattern.

In addition, we investigate the distribution of mask sizes in SAMRS, as shown in Figure 5. The results indicate that, in general, there are more instances with smaller sizes in all subsets. However, some differences exist between the

subsets. Specifically, FAST has more small objects than the other two sets. Nevertheless, SOTA appears to have a higher number of extremely small targets (*i.e.*, <100 pixels), since its source dataset DOTA-V2.0 is designed for small object detection. On the other hand, SIOR has a more smooth distribution of mask sizes compared to SOTA and FAST.

### 3.3. Visualization

In Figure 6, we visualize some segmentation annotations from the three subsets in our SAMRS dataset. As can be seen, SOTA exhibits a greater number of instances for tiny cars, whereas FAST provides a more fine-grained annotation of existing categories in SOTA such as car, ship, and plane. SIOR on the other hand, offers annotations for more diverse ground objects, such as *dam*. Hence, our SAMRS dataset encompasses a wide range of categories with varying sizes and distributions, thereby presenting a new challenge for RS semantic segmentation.

## 4. Conclusion

This study showcases an effective way to create a large-scale remote sensing (RS) segmentation dataset by leveraging the Segment Anything Model (SAM) and existing object detection datasets. Given the unique characteristics of RS data labeling, we explore the performance of various prompts to determine the optimal settings for SAM. Based on the optimal settings, we obtain massive mask annotations for RS images, resulting in the creation of a large-scale segmentation dataset named SAMRS, which surpasses all previous high-resolution RS segmentation datasets in volume. In addition, our statistical analysis shows that SAMRS contains a wide range of categories with varying sizes and distributions. SAMRS can be utilized for semantic segmentation, instance segmentation, and object detection studies, either individually or in combination, particularly in the context of large model pre-training.

## Acknowledgement

We acknowledge the authors of SAM for releasing codes and models, and the authors of DOTA, DIOR, and FAIR1M for providing their datasets.

## Appendix

For the SOTA dataset, we present the list of all category abbreviations as follows. *LV*: large vehicle, *SP*: swimming pool, *HC*: helicopter, *BR*: bridge, *PL*: plane, *SH*: ship, *SBF*: soccer ball field, *BC*: basketball court, *GTF*: ground track field, *SV*: small vehicle, *BD*: baseball diamond, *TC*: tennis court, *RA*: roundabout, *ST*: storage tank, *HA*: harbor, *CC*: container crane, *AP*: airport, *HP*: helipad.

For the SIOR dataset, we present the list of all category abbreviations as follows. *APL*: airplane, *APO*: airport, *BF*: baseballfield, *BC*: basketballcourt, *BR*: bridge, *CH*: chimney, *ESA*: expressway service area, *ETS*: expressway toll station, *DA*: dam, *GF*: golffield, *GTF*: groundtrackfield, *HA*: harbor, *OP*: overpass, *SH*: ship, *STD*: stadium, *STT*: storagetank, *TC*: tenniscourt, *TS*: trainstation, *VH*: vehicle, *WD*: windmill.

For the SIOR dataset, we present the list of all category abbreviations as follows. *A2*: A220, *A3*: A321, *A4*: A330, *A5*: A350, *ARJ*: ARJ21, *BF*: baseball field, *BC*: basketball court, *B3*: boeing737, *B4*: boeing747, *B7*: boeing777, *B8*: boeing787, *BR*: bridge, *BU*: bus, *C9*: C919, *CT*: cargo truck, *DCS*: dry cargo ship, *DT*: dump truck, *ES*: engineering ship, *EV*: excavator, *FB*: fishing boat, *FF*: football field, *IN*: intersection, *LCS*: liquid cargo ship, *MB*: motorboat, *OA*: other airplane, *OS*: other ship, *OV*: other vehicle, *PS*: passenger ship, *RA*: roundabout, *SC*: small car, *TC*: tennis court, *TRT*: tractor, *TRL*: trailer, *TUT*: truck tractor, *TB*: tugboat, *VA*: van, *WS*: warship.

## References

- [1] Fair1m: A benchmark dataset for fine-grained object recognition in high-resolution remote sensing imagery. *ISPRS Journal of Photogrammetry and Remote Sensing*, 184:116–130, 2022.
- [2] Adrian Boguszewski, Dominik Batorski, Natalia Ziembajankowska, Tomasz Dziedzic, and Anna Zambrzycka. Landcover. ai: Dataset for automatic mapping of buildings, woodlands, water and roads from aerial imagery. In *Proceedings of the IEEE/CVF Conference on Computer Vision and Pattern Recognition*, pages 1102–1110, 2021.
- [3] Ilke Demir, Krzysztof Koperski, David Lindenbaum, Guan Pang, Jing Huang, Saikat Basu, Forest Hughes, Devis Tuia, and Ramesh Raskar. Deepglobe 2018: A challenge to parse the earth through satellite images. In *Proceedings of the IEEE Conference on Computer Vision and Pattern Recognition Workshops*, pages 172–181, 2018.
- [4] Ruining Deng, Can Cui, Quan Liu, Tianyuan Yao, Lucas W Remedios, Shunxing Bao, Bennett A Landman, Lee E Wheless, Lori A Coburn, Keith T Wilson, et al. Segment anything model (sam) for digital pathology: Assess zero-shot segmentation on whole slide imaging. *arXiv preprint arXiv:2304.04155*, 2023.
- [5] Jian Ding, Nan Xue, Gui-Song Xia, Xiang Bai, Wen Yang, Michael Yang, Serge Belongie, Jiebo Luo, Mihai Datcu, Marcello Pelillo, and Liangpei Zhang. Object detection in aerial images: A large-scale benchmark and challenges. *IEEE Transactions on Pattern Analysis and Machine Intelligence*, pages 1–1, 2021.
- [6] Alexander Kirillov, Eric Mintun, Nikhila Ravi, Hanzi Mao, Chloe Rolland, Laura Gustafson, Tete Xiao, Spencer Whitehead, Alexander C. Berg, Wan-Yen Lo, Piotr Dollár, and Ross Girshick. Segment anything. *arXiv:2304.02643*, 2023.
- [7] Ke Li, Gang Wan, Gong Cheng, Liqiu Meng, and Junwei Han. Object detection in optical remote sensing images: A survey and a new benchmark. *ISPRS journal of photogrammetry and remote sensing*, 159:296–307, 2020.
- [8] Zikun Liu, Liu Yuan, Lubin Weng, and Yiping Yang. A high resolution optical satellite image dataset for ship recognition and some new baselines. In *ICPRAM*, pages 324–331, 2017.
- [9] Ye Lyu, George Vosselman, Gui-Song Xia, Alper Yilmaz, and Michael Ying Yang. Uavid: A semantic segmentation dataset for uav imagery. *ISPRS journal of photogrammetry and remote sensing*, 165:108–119, 2020.
- [10] Jun Ma and Bo Wang. Segment anything in medical images. *arXiv preprint arXiv:2304.12306*, 2023.
- [11] Diego Marcos, Michele Volpi, Benjamin Kellenberger, and Devis Tuia. Land cover mapping at very high resolution with rotation equivariant cnns: Towards small yet accurate models. *ISPRS journal of photogrammetry and remote sensing*, 145:96–107, 2018.
- [12] Xin-Yi Tong, Gui-Song Xia, Qikai Lu, Huanfeng Shen, Shengyang Li, Shucheng You, and Liangpei Zhang. Landcover classification with high-resolution remote sensing images using transferable deep models. *Remote Sensing of Environment*, 237:111322, 2020.

- [13] Michele Volpi and Vittorio Ferrari. Semantic segmentation of urban scenes by learning local class interactions. In *Proceedings of the IEEE Conference on Computer Vision and Pattern Recognition Workshops*, pages 1–9, 2015.
- [14] Di Wang, Jing Zhang, Bo Du, Gui-Song Xia, and Dacheng Tao. An empirical study of remote sensing pretraining. *IEEE Transactions on Geoscience and Remote Sensing*, 2022.
- [15] Di Wang, Qiming Zhang, Yufei Xu, Jing Zhang, Bo Du, Dacheng Tao, and Liangpei Zhang. Advancing plain vision transformer towards remote sensing foundation model. *IEEE Transactions on Geoscience and Remote Sensing*, 2022.
- [16] Junjue Wang, Zhuo Zheng, Ailong Ma, Xiaoyan Lu, and Yanfei Zhong. Loveda: A remote sensing land-cover dataset for domain adaptive semantic segmentation. *arXiv preprint arXiv:2110.08733*, 2021.
- [17] Syed Waqas Zamir, Aditya Arora, Akshita Gupta, Salman Khan, Guolei Sun, Fahad Shahbaz Khan, Fan Zhu, Ling Shao, Gui-Song Xia, and Xiang Bai. isaid: A large-scale dataset for instance segmentation in aerial images. In *Proceedings of the IEEE Conference on Computer Vision and Pattern Recognition Workshops*, pages 28–37, 2019.
- [18] Gui-Song Xia, Xiang Bai, Jian Ding, Zhen Zhu, Serge Belongie, Jiebo Luo, Mihai Datcu, Marcello Pelillo, and Liangpei Zhang. Dota: A large-scale dataset for object detection in aerial images. In *The IEEE Conference on Computer Vision and Pattern Recognition (CVPR)*, June 2018.